

HIGHLIGHT

Oxygen Transport as a Solid-State Structure Probe for Polymeric Materials: A Review

A. HILTNER, R. Y. F. LIU, Y. S. HU, E. BAER

Department of Macromolecular Science and Center for Applied Polymer Research, Case Western Reserve University, Cleveland, Ohio 44106-7202

Received 11 August 2004; Revised 1 November 2004; Accepted 14 November 2004

DOI: 10.1002/polb.20349

Published online in Wiley InterScience (www.interscience.wiley.com).

ABSTRACT: In the quest to elucidate the solid-state structures of polymers, insight into the amorphous phase is particularly elusive. Although the permeability of small molecules is often measured as an important performance property, numerous researchers have found that a deeper analysis of the transport characteristics provides insight into polymer morphology, especially if used in combination with more usual characterization techniques. The transport of small gas molecules senses the permeable amorphous structure and probes the nature of

the free volume. In recent years, our interest in the gas barrier of polyesters has resulted in an unusual opportunity to investigate the nature of the free volume in the polymer glassy state. This effort has been aided by access to aromatic polyesters with designed variations in their chemical structure. This review focuses on oxygen transport, supplemented with other methods of physical analysis, as a probe of the excess-hole free volume. The review addresses the profound effects of orientation and crystallization on the free volume of the glassy state. The

discussion also presents a simple model for the gas permeability of the isotropic glass based on lattice concepts and tests more sophisticated models for the gas permeability of semicrystalline polymers. The final section addresses other opportunities for fruitful applications of oxygen transport as a solid-state structure probe. © 2005 Wiley Periodicals, Inc. *J Polym Sci Part B: Polym Phys* 43: 1047–1063, 2005

Keywords: crystallization; dedensification; densification; diffusion; free volume; liquid crystallinity; orientation; oxygen transport



ANNE HILTNER

Anne Hiltner received her BA from Reed College in Portland, Oregon, and her PhD from Oregon State University working with Wendell Slabaugh on swelling of alkylammonium montmorillonites. She has been on the faculty of Case Western Reserve University since 1974 and currently holds the Herbert Henry Down Professorship of Science and Engineering. Her research collaborations with Eric Baer focus on the areas of structure-property-processing relationships in polymers; irreversible deformation, crack propagation and fracture; nanolayered polymers by forced assembly; gas transport in polymers; and biostability of polymeric biomaterials.

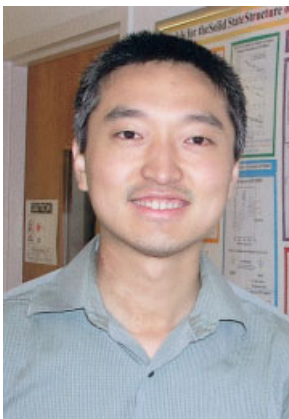
Correspondence to: A. Hiltner (E-mail: pah6@case.edu)

Journal of Polymer Science: Part B: Polymer Physics, Vol. 43, 1047–1063 (2005)
© 2005 Wiley Periodicals, Inc.



**RICHARD YUFENG
LIU**

Richard Yufeng Liu received his PhD degree in macromolecular science from Case Western Reserve University in 2005 and a Bachelors degree in polymer chemical engineering from Sichuan University in 1999. Under the direction of his advisors, Anne Hiltner and Eric Baer, he focused his research on understanding gas transport mechanisms in glassy and oriented polymers in monolithic and multilayer constructions. He is currently employed by 3M.



YUSHAN HU

Yushan Hu received his BS in the Department of Chemistry in 1997 and MS in the Institute of Polymer Chemistry in 2000 from Nankai University. He is currently completing his PhD at Case Western Reserve University under the supervision of Anne Hiltner and Eric Baer. His studies include gas transport properties of polymers, phase separation in polymer blends, and morphology of liquid crystalline polyester.



ERIC BAER

Eric Baer received his MS and DEng degrees from Johns Hopkins University. After terms at DuPont and the University of Illinois, he joined the faculty of Case Western Reserve University in 1962 where he founded the Department of Macromolecular Science and Engineering. Currently, as the Leonard Case Professor of Engineering, he applies hierarchical concepts and bioinspiration to a variety of polymeric materials systems.

INTRODUCTION

Background

The permeability of polymers to gases and liquids has been recognized for many years as an important performance property that is routinely evaluated for a variety of applications in the packaging and separation industries. However, the concept of using small molecules to probe solid-state structures can be dated to 1961, when Michaels and Bixler¹ stated the following:

An important aspect of this study which must not be overlooked is the insight into polymer morphology gained from analysis of the diffusion process. Use of diffusing gases as molecular 'probes' tends to supplement data obtained from more conventional sources such as X-ray analysis, electron microscopy, and light-scattering.

The development of this concept over subsequent decades is expressed in a 1985 comment of Rogers:²

An objective of research in this field is to establish mechanisms and expressions relating solubility and transport with the molecular properties and characteristics of the components. Conversely, the nature of the solution and diffusion processes can help elucidate inherent characteristics of the polymeric material such as the flexibility and conformation of the chain segments, interactions and structural and morphological features. This is the 'molecular probe' aspect which has been employed to advantage in conjunction with more usual characterization techniques.

The concept attained widespread acceptance by 1991 when Vieth³ was able to state the following:

Having already obtained a reasonable degree of success in interpreting the microstructure of semicrystalline and glassy polymers via these (sorption and transport) properties, the use of small molecules as micro-structural probes is being more and more enthusiastically adopted by chemical engineers and chemists who are involved in applied research on polymeric materials.

Among the many examples that attest to the value of gas transport as a solid-state probe, specific references have been made to the following contributions:

- Barrie et al.⁴ on the dual-sorption mode, which defines two concurrent mechanisms of sorption in glassy polymers: bulk dissolution according to Henry's law and filling holes of free volume.
- Michaels and coworkers^{1,5,6} on the use of gas transport to probe the crystalline and amorphous phases of semicrystalline polymers.

- Koros and coworkers⁷⁻⁹ on the generalization of the dual-sorption model with extension to dual diffusion and permeation models.
- Meares¹⁰ on the mechanistic interpretation of activated gas diffusion.
- Paul and coworkers¹¹⁻¹³ on the gas-transport mechanism of liquid-crystalline polymers (LCPs).
- Ward and coworkers¹⁴⁻¹⁶ on the gas-transport properties in oriented polymers.
- Freeman and others¹⁷⁻¹⁹ on the use of organic vapor and liquid sorption to probe the dedensification of polyesters by solvent-induced crystallization.

In recent years, our interest in the gas barrier of polyesters has resulted in an unusual opportunity to investigate the nature of the free volume in the polymer glassy state. This effort has been aided by the availability of commercial gas-transport instruments with excellent sensitivity and by access to aromatic polyesters with designed variations in their chemical structure. This review focuses on oxygen transport, supplemented with other methods of physical analysis, as a probe of the excess-hole free volume. The review addresses the profound effects of orientation and crystallization on the free volume of the glassy state. The discussion presents a simple model for the gas permeability of the isotropic glass based on lattice concepts and tests more sophisticated models for the gas permeability of semicrystalline polymers. The final section addresses other opportunities for fruitful applications of oxygen transport as a solid-state structure probe.

Transport Measurements

The rate of gas permeation through a polymer film is determined by the permeability (P), which is a product of a kinetic parameter, the diffusivity (D), and a thermodynamic parameter, the solubility (S):

$$P = DS \quad (1)$$

Although P measures the steady-state flux and is of considerable practical importance, fundamental insight into the gas-transport process is provided by D and S . To obtain P , D , and S , we measure the oxygen flux [$J(t)$] at a constant temperature and a constant relative humidity with commercial instruments (Mocon) that employ the continuous-flow cell method. A mixture of 98% N_2 and 2% H_2 is the carrier gas; the test gas is 100% O_2 or alternatively a mixture of O_2 with N_2 if a lower O_2 pressure is desired.

Figure 1 shows a typical experimental $J(t)$ curve for a poly(ethylene terephthalate) (PET) film. Careful outgassing and the appropriate choice of the specimen thick-

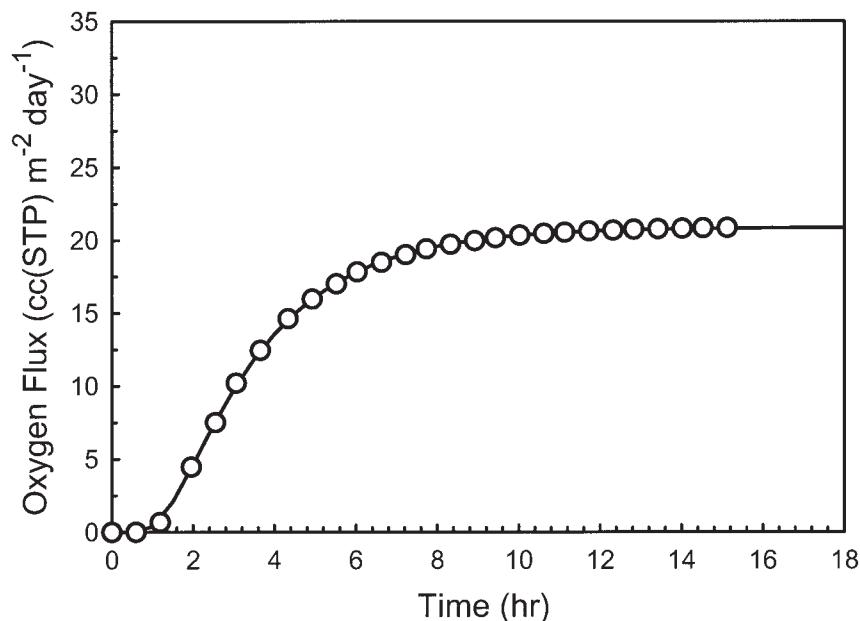


Figure 1. Experimental $J(t)$ data for glassy PET at 23 °C and the fit to eq 3.

ness result in the excellent resolution of the various features of the time dependence. The initial increase in $J(t)$ reflects the non-steady-state process of oxygen penetration into the film. This part of the curve is determined mainly by D . As the oxygen concentration in the film reaches a constant distribution, the flux levels out and approaches the steady-state value J , which, normalized by the film thickness (l) and the oxygen pressure (p), defines P as $P = Jl/p$.

To obtain D and to accurately determine P , we fit the flux to the solution of Fick's second law:

$$\frac{\partial c}{\partial t} = D \frac{\partial^2 c}{\partial x^2} \quad (2)$$

With the oxygen-concentration boundary conditions $c(x = 0, t) = Sp$ and $c(x = l, t) = 0$ and the initial condition $c(x, t = 0) = 0$,^{20,21} we obtain

$$J(t) = \frac{Pp}{l} \left[1 + 2 \sum_{n=1}^{\infty} (-1)^n \exp\left(-\frac{D\pi^2 n^2 t}{l^2}\right) \right] \quad (3)$$

By fitting the flux–time curve, we can extract both P and D . Subsequently, S is calculated according to eq 1. The fitting curve is included with the experimental points in Figure 1. From the quality of the fit, we can conclude that there is no concentration dependence of D for oxygen at 1 atm. The fit is equally good for all the measurements reported. The main source of error in calculating P and D from the experimental flux curve lies in the determina-

tion of l . Some thickness variation is inherent to all films, especially to those prepared in the laboratory by compression molding. If the thickness variation is less than 30%, the accuracy of P and D is determined mainly by the accuracy of the average thickness measurement. A convenient and accurate method is to weigh the tested area and to calculate the average thickness as $l = W/(A\rho)$, where W is the specimen weight, A is the specimen area, and ρ is the density.

GLASSY POLYESTERS

Oxygen Solubility and Free Volume

As a result of the long timescale required for glassy polymers to relax fully, the volume of the nonequilibrium glassy polymer is larger than the volume extrapolated from equilibrium by the excess-hole free volume (Fig. 2).²² The amount of excess-hole free volume in a typical glassy polymer such as PET, often defined as the fractional free volume (FFV), is approximately 0.036.^{23,24} The excess-hole free volume is thought to be distributed in the form of small holes throughout the glass. Findings from positron annihilation lifetime spectroscopy (PALS) suggest that the hole radius in PET is approximately 0.26 nm, and the density of holes is about $4 \times 10^{20} \text{ cm}^{-3}$.^{25,26} However, FFV can be as high as 0.28 and the hole radius can be as high as 0.5 nm in the so-called high-free-volume polymer glasses.²⁷

Oxygen molecules sorbed in a glassy polymer at a low pressure are viewed as filling holes of free volume.²⁸ Gas

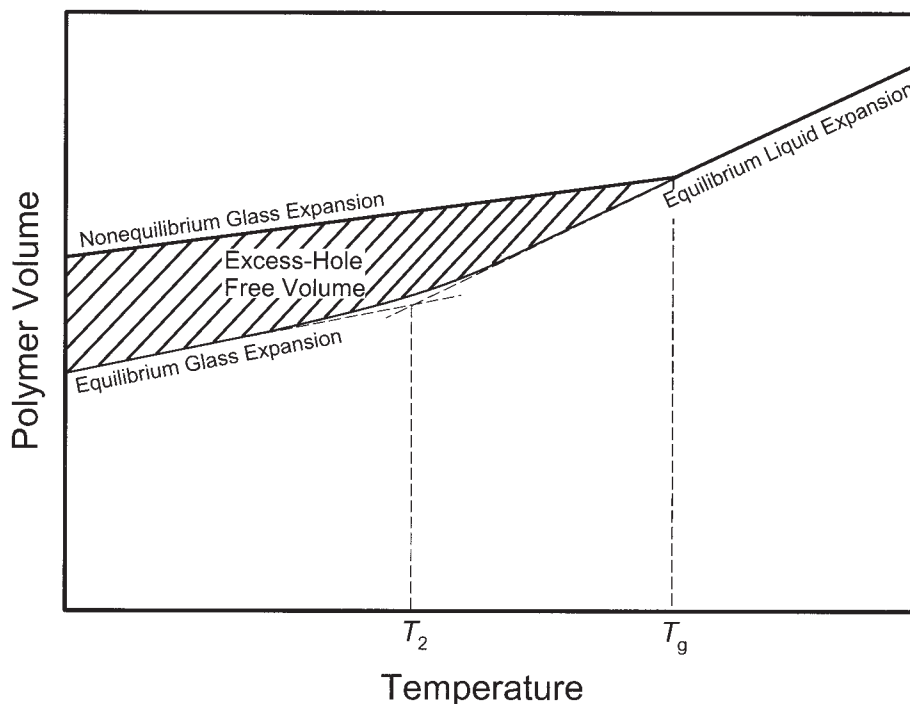


Figure 2. Schematic representation of the volume–temperature relationship for an amorphous polymer following the concepts of Vrentas and Duda.²²

permeation proceeds by jumps through the excess-hole free volume. In simplified terms,²⁹ the permeant gas molecule spends most of the time in free-volume holes and occasionally jumps into a neighboring hole. The jump motion proceeds by the formation of a channel between two neighboring holes.³⁰ Thus, gas permeation depends on the number and size of the holes in the polymer matrix (static free volume) and the frequency of channel formation (dynamic free volume). Static free volume is essentially independent of the thermally accessible motions of the macromolecules and is related to gas solubility. Dynamic free volume derives from accessible conformational changes and segmental motions of the macromolecule and is related to gas diffusivity.

According to free-volume concepts, the excess-hole free volume decreases as the glassy polymer approaches the glass-transition temperature (T_g). This is the basis for the relationship between S for oxygen and T_g in Figure 3.²⁶ S , measured at the test temperature (T_{test}), is plotted versus the temperature difference from T_g , that is, the quantity $T_g - T_{\text{test}}$, for a series of glassy copolymers based on PET.^{24,31} In this case, S was measured primarily at $T_{\text{test}} = 25^\circ\text{C}$, and the polyesters differed in T_g . The right branch of the plot in the temperature region of $20^\circ\text{C} \leq T_g - T_{\text{test}} \leq 60^\circ\text{C}$ shows a linear decrease in S as T_g approaches T_{test} , and this reflects the reduction of the excess-hole free volume. Extrapolation gives zero solubility at $T_g = T_{\text{test}}$, at which point the excess-hole free volume is expected to disappear.²² The slope (β_1) gives

the density of sorbed oxygen (ρ_{O_2}) in the free-volume holes at T_{test} .²⁴

$$\rho_{\text{O}_2} = \frac{\nu\beta_1}{\Delta e} \left(\frac{M_w}{22,400} \right) \quad (4)$$

where ν is the specific volume of the polymer ($0.749\text{ cm}^3\text{ g}^{-1}$ for glassy PET), Δe is the difference in the thermal expansivity of the rubbery and glassy states ($4.8 \times 10^{-4}\text{ cm}^3\text{ g}^{-1}\text{ K}^{-1}$ for PET),³² and M_w is the weight-average molecular weight (32 for oxygen). ρ_{O_2} is $3.8 \times 10^{-3}\text{ g/cm}^3$ of free volume or about 3 atm, and this indicates that sorbed oxygen is in the gaseous state. For $T_g > T_{\text{test}} + 60^\circ\text{C}$, the decreasing slope of the relationship between S and $T_g - T_{\text{test}}$ suggests that the excess-hole free volume approaches a constant value at temperatures well below T_g . The aromatic polyesters appear to approach a constant FFV of about 0.05 below the proposed second-order transition at approximately $T_g - 60^\circ\text{C}$.^{24,33,34}

As the glassy polymer approaches T_g , Henry's law sorption is no longer negligible. Results for some low- T_g amorphous aromatic copolyesters based on diethylene glycol and results for poly(diethylene glycol isophthalate) (PDEGI) at T_{test} from -11 to 40°C extend the plot into the rubbery region, as reflected by the left branch in Figure 3. The inclusion of data obtained at temperatures other than 25°C assumes that ρ_{O_2} does not change very much over a small temperature range. A deviation from

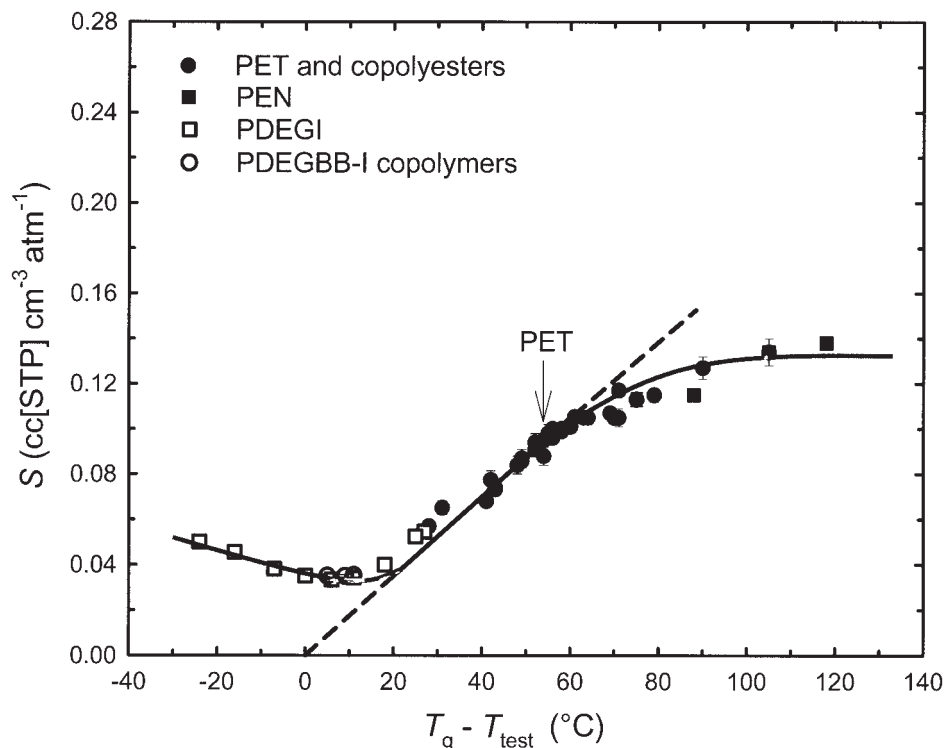


Figure 3. Relationship between S for oxygen and $T_g - T_{\text{test}}$.²⁶ Reprinted with permission from Hu, Y. S.; Liu, R. Y. F.; Schiraldi, D. A.; Hiltner, A.; Baer, E. *Macromolecules* 2004, 37, 2136. Copyright 2004 American Chemical Society.

the linear relationship between S and $T_g - T_{\text{test}}$ due to Henry's law sorption begins about 20 °C below T_g , and this attests to the considerable breadth of the glass-transition region. Once the polymer reaches the rubbery state, S gradually increases with temperature.

It follows from the free-volume interpretation of S that a relationship exists between S and ν .²⁴ The relationship is tested with copolymers of PET with isomeric isophthalic acid and phthalic acid in Figure 4. The linear relationship is

$$S = \beta(\nu - \nu_0) \quad (5)$$

where ν_0 is the specific volume of the polymer with $S = 0$ and, therefore, represents the equilibrium specific volume of the glassy polymer with no excess-hole free volume. In eq 5, the slope [$\beta = 3.6 \text{ cc (STP) g cm}^{-6} \text{ atm}^{-1}$] reflects ρ_{O_2} in the excess-hole free volume:

$$\rho_{\text{O}_2} = \frac{\nu\beta p M_w}{22,400} \quad (6)$$

where ν is the specific volume of the glassy polymer, p is 1 atm, and $M_w = 32 \text{ g mol}^{-1}$ is the molecular weight of oxygen. Equation 6 yields a ρ_{O_2} value of approximately $3.9 \times 10^{-3} \text{ g/cm}^3$ of free volume or about 3 atm,

the same value extracted from the relationship between S and T_g according to eq 4.

From ν_0 (the specific volume of the polymer at the equilibrium condition with zero accessible free volume) and β (which is related to ρ_{O_2} according to eq 6), the specific excess-hole free volume of the glassy polymer (ν_f) is

$$\nu_f = \nu - \nu_0 = \frac{S}{\beta} \quad (7)$$

Alternatively, FFV can be calculated readily from S for oxygen:

$$\text{FFV} = \frac{\nu_f}{\nu} = \frac{S}{\beta\nu} \quad (8)$$

These results can be tested against other methods for probing the free volume, such as PALS.

Temperature–Volume Relationship

It is now possible to construct the volume–temperature behavior of an amorphous polymer by using the oxygen solubility to measure the excess-hole free volume. The

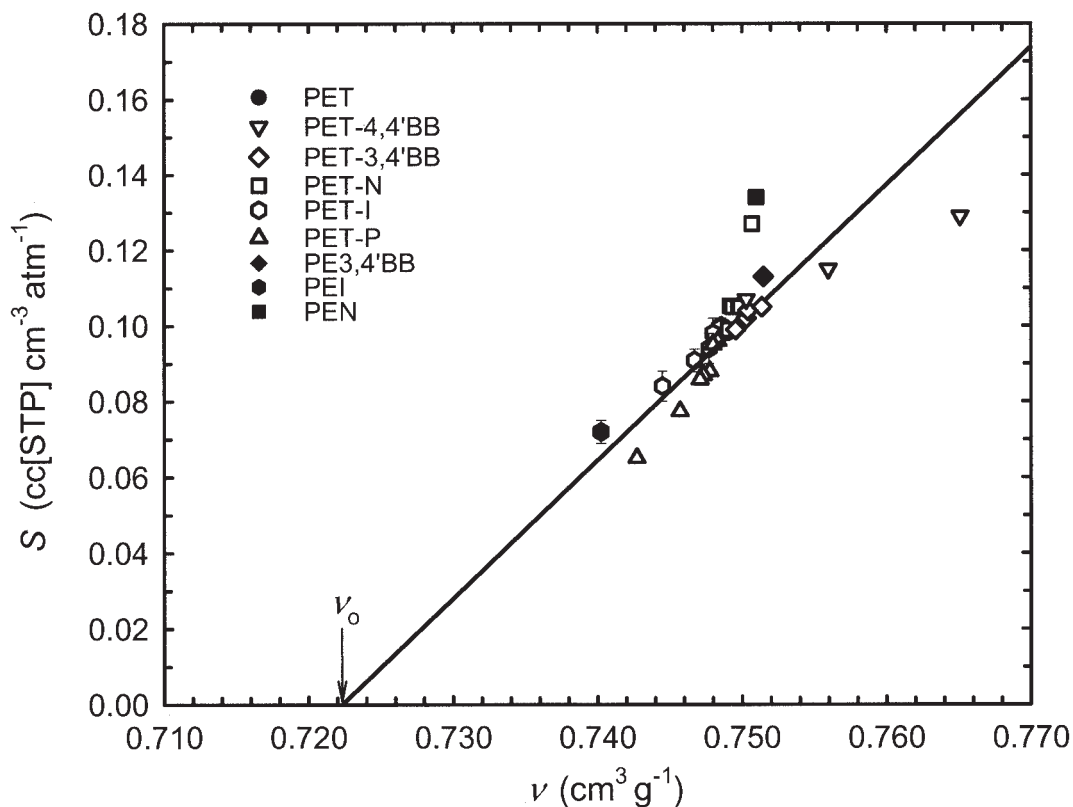


Figure 4. Relationship between S for oxygen and ν for glassy copolyesters based on PET. The linear correlation extrapolates to $S = 0$ at $\nu_0 = 1.38 \text{ g cm}^{-3}$, the density of the amorphous polymer with no excess-hole free volume, with a slope of $\beta = 3.6 \text{ cc (STP) g cm}^{-6} \text{ atm}^{-1.24}$

example in Figure 5 is for PET. The $\nu(T)$ line of the amorphous glass is constructed from the reference point defined by the amorphous density of 1.335 g cm^{-3} at $25 \text{ }^\circ\text{C}$ and by the T_g value of $81 \text{ }^\circ\text{C}$. The specific thermal expansion coefficients, e_g and e_l , are taken to be 2.2 and $7.0 \times 10^{-4} \text{ cm}^3 \text{ g}^{-1} \text{ K}^{-1}$, respectively.³² Reported experimental values and group-contribution calculations reveal similar values of e_g and e_l for the aromatic polyesters based on ethylene terephthalate.³² Therefore, it is possible to superimpose the thermal expansion of all the aromatic polyesters with respect to that of PET, and they should overlap. The x axis is the temperature with respect to T_g ($T_{\text{test}} - T_g$). This allows us to expand the temperature range by incorporating data for various aromatic polyesters that differ in T_g . For each data point in Figure 5, ν_f is calculated from eq 7 and subtracted from the amorphous glass line of PET at the appropriate value of $T_{\text{test}} - T_g$. Consistency in ν_f among the different aromatic polyesters reflects the common characteristics of excess-hole free volume in the glassy state.

The curve through the open circles in Figure 5 extends the equilibrium liquid line below T_g . In agreement with the model in Figure 2, the excess-hole free volume becomes less dependent on the temperature for $T_{\text{test}} - T_g < -60 \text{ }^\circ\text{C}$ and indeed appears to approach a constant

value of approximately $0.04 \text{ cm}^3 \text{ g}^{-1}$ (FFV ~ 0.05). The coincidence of the slope change with the postulated second-order transition at $T_g - 60 \text{ }^\circ\text{C}$ ^{33,34} suggests that at temperatures below $T_g - 60 \text{ }^\circ\text{C}$, gas solubility probes the core expansion of the equilibrium glassy state. In this interpretation, the supercooled glass follows the equilibrium liquid-expansion line between T_g and $T_g - 60 \text{ }^\circ\text{C}$ and exhibits constant free volume below the transition in agreement with the classical Williams–Landel–Ferry interpretation.³⁵

Decreasing Free Volume by Orientation

The orientation of PET and other aromatic polyesters by cold drawing below T_g significantly increases the density even though strain-induced crystallization is prevented. The processes of orientation and densification correlate with the conformational transformation of glycol linkages from gauche to trans. Correspondingly, oxygen permeability is reduced because of decreases in both D and S .^{23,25,36} The decrease in S for three cold-drawn polyesters is plotted versus ν according to eq 7 in Figure 6. For PET, the linear relationship coincides with that of PET-based copolymers in Figure 4 and indicates that the

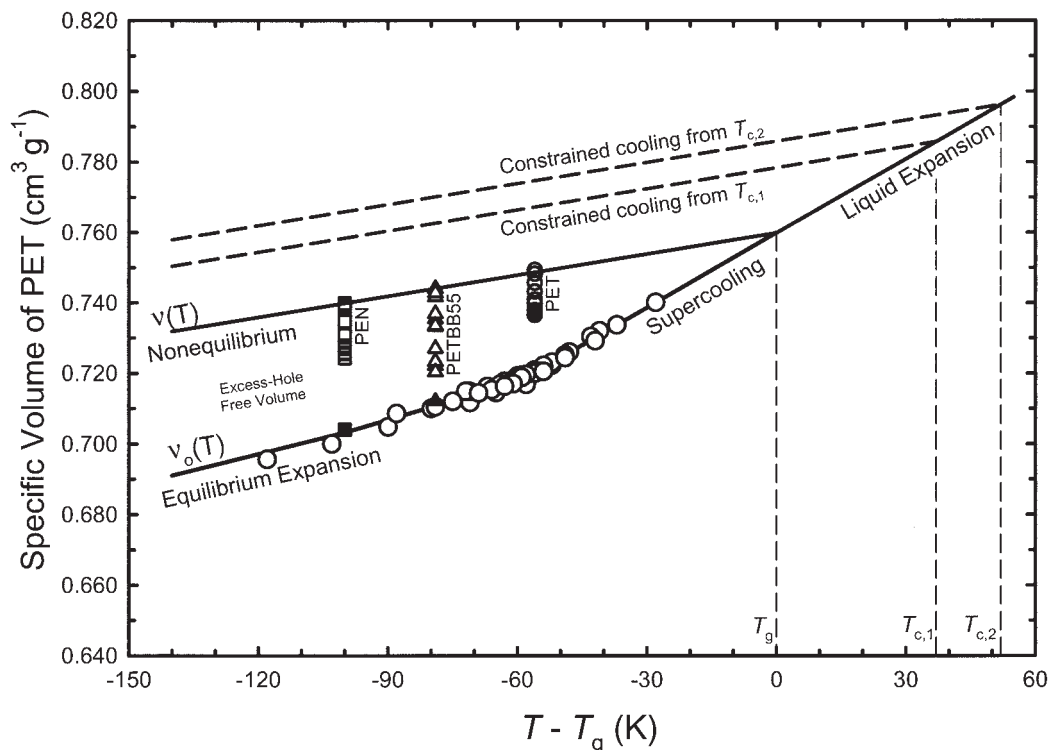


Figure 5. Relationship between ν and $T - T_g$, constructed for amorphous PET with the oxygen solubility as a measure of the accessible free volume and including data for various copolymers,²⁴ the effect of orientation,²³ and the effect of constraint on the spherulite amorphous phase.⁵⁸ Reprinted with permission from Hu, Y. S.; Liu, R. Y. F.; Zhang, L. Q.; Rogunova, M.; Schiraldi, D. A.; Nazarenko, S.; Hiltner, A.; Baer, E. *Macromolecules* 2002, 35, 7326. Copyright 2002 American Chemical Society.

decrease in S arises from the reduction in the excess-hole free volume. Despite differences in the chemical structure, a β value of about 3.6 has been obtained for each of the polymers, and this suggests that the physical state of sorbed oxygen is the same in all the polyesters. On the other hand, a different value of ν_0 for each polyester means that the specific volume at zero solubility is characteristic of the chemical structure. Very low gas solubility is characteristic of LCPs. It is instructive that the point for Vectra, an LCP with a high percentage of naphthalate units, is very close to ν_0 of poly(ethylene naphthalate) (PEN).

The orientation effect is incorporated into the volume-temperature relationship in Figure 5. At the appropriate value of $T_{\text{test}} - T_g$, ν_0 from Figure 6 lies on the equilibrium expansion curve determined for glassy copolyesters. Gradually reducing the excess-hole free volume by orientation produces a series of points that bring the nonequilibrium glass closer to the equilibrium line. A cold-drawn copolymer based on PET with 55 mol % of the terephthalate replaced with 4,4'-biphenylate (PETBB55) approaches the zero-solubility condition most closely, perhaps because the liquid-crystalline (LC)-like character of this polymer facilitates orientation.³⁷

Oxygen Diffusivity and Molecular Relaxation

The dynamic free volume that controls the jump motion of permeant molecules between static free-volume holes derives from accessible conformational changes and segmental motions of the polymer chain. For glassy polyesters, it appears that these thermal rearrangements are manifest in the sub- T_g γ -relaxation process.³⁸ The diffusivity of copolyesters based on PET shows an excellent logarithmic dependence on the relative relaxation intensity, which is defined as $1 - (I_{E''}/I_{E'',\text{PET}})$, where $I_{E''}$ is the relaxation intensity taken as the area under the log E'' curve, where E'' is the loss modulus, and $I_{E'',\text{PET}}$ is the relaxation intensity of PET (Fig. 7). Further evidence that the dynamic free volume for oxygen diffusion arises from the same thermally activated motions of glycol conformations as the γ relaxation is provided by the correspondence between the activation energy for oxygen diffusion (E_D) and the activation energy of the γ relaxation (E_γ) (Table 1).³⁹⁻⁴² Results for numerous other aromatic polyesters, including poly(diethylene glycol 4,4'-biphenylate) (PDEGBB),⁴³ poly(diethylene glycol 4,4'-biphenylate-*co*-isophthalate) copolymers (PDEGBB-I),²⁶ and poly[ethylene-*co*-bis(2-hydroxyethyl)hydroquinone terephthalate]

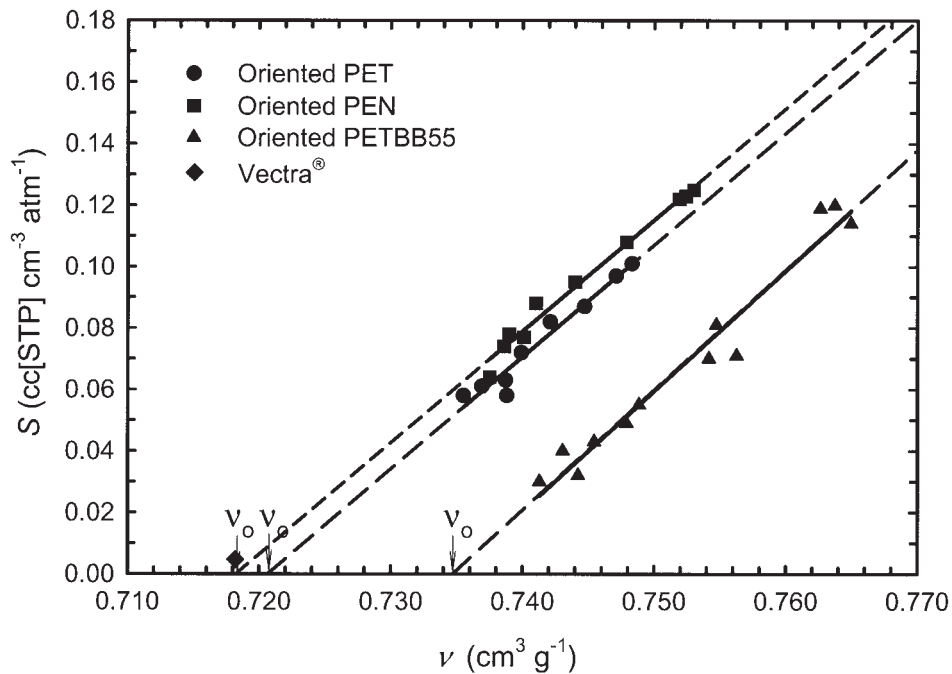


Figure 6. Effect of the orientation on the relationship between S for oxygen and ν . The linear correlation extrapolates to a different value of ν_0 at $S = 0$ for each polymer but with the same slope of $\beta = 3.6 \text{ cc (STP) g cm}^{-6} \text{ atm}^{-1}$.²³

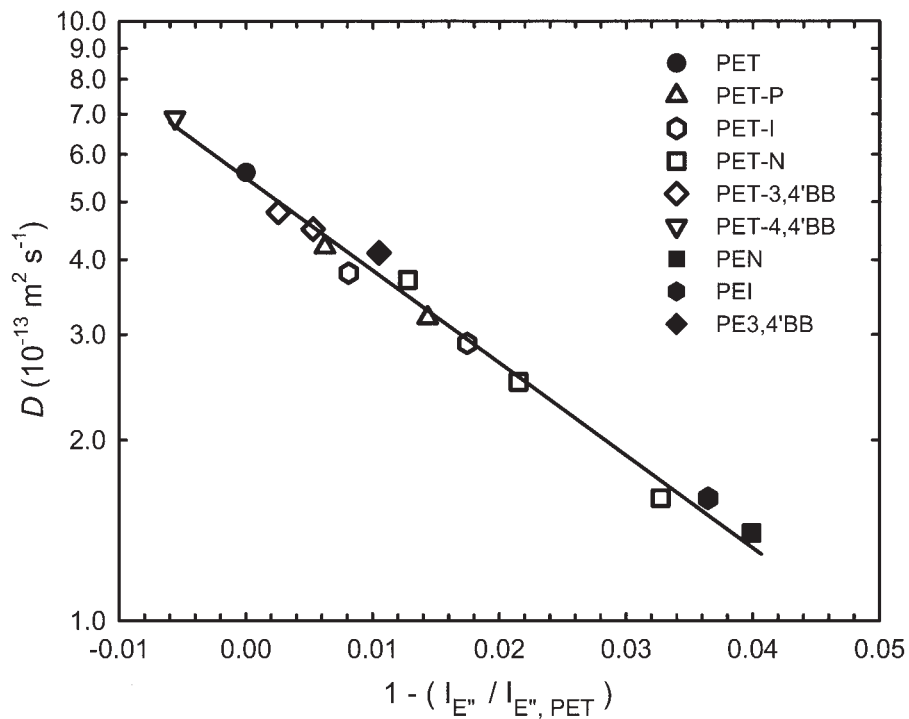


Figure 7. Relationship between D for oxygen and the relative intensity of the γ relaxation.²⁴

Table 1. Properties of Glassy Polyesters

Property	PEN	PETBB55	PET	PEI	PDEGBB (LC)
ρ at 25 °C (g cm ⁻³)	1.3272	1.3080	1.3359	1.3509	1.3201
T_g (°C)	124	104	79	68	42
P at 25 °C [cc (STP) cm m ⁻² day ⁻¹ atm ⁻¹]	0.167	0.650	0.463	0.099	0.0318
D at 25 °C (10 ⁻¹³ m ² s ⁻¹)	1.6	6.6	5.2	1.6	2.6
S at 25 °C [cc (STP) cm ⁻³ atm ⁻¹]	0.121	0.114	0.103	0.072	0.014
FFV at 25 °C	0.049	0.039	0.038	0.027	0.005
E_D (kJ mol ⁻¹)	44	43	40	43	53
E_γ (kJ mol ⁻¹)	58.2	—	49.8	56.9	—
			52.1 (trans)		
			32.8 (gauche)		
CED (10 ⁸ J m ⁻³)	5.3	5.3	5.4	5.5	5.2
α (Å)	14.5	14.2	12.9	13.7	18
r at 25 °C (Å, PALS)	2.59	2.58	2.56	2.41	2.23
r_m at 25 °C (Å, eq 10)	3.1	2.9	2.8	2.5	1.9

copolymers,⁴⁴ demonstrate the generality of the relationship between the γ -relaxation strength and oxygen diffusivity.

The complexity of the γ relaxation has sometimes led investigators to identify specific components with trans and gauche conformers of the glycol,⁴⁵ with somewhat different activation energies.⁴² Some γ -relaxation motions may be more effective than others for enabling the jump motion of permeant molecules between static free-volume cavities. An increase in gauche conformers has been linked to higher oxygen permeability.^{14,15} For example, the gauche fraction from infrared spectroscopy is 0.91 for PET and 0.93 for PETBB55, but it is only 0.75 for poly(ethylene isophthalate) (PEI) and 0.79 for PEN, which have much lower diffusivity.^{23,25} Apparently, motions of gauche glycol conformations provide the dynamic free volume associated with diffusivity. Indeed, a better correlation between the diffusivity and relaxation intensity is obtained if only the gauche component of the γ relaxation is considered.³¹

Lattice Hole Model for Gas Permeation

The interpretation of oxygen solubility and diffusivity in terms of static and dynamic free-volume concepts leads to a very simple lattice model for oxygen transport. Spherical holes of excess-hole free volume having radius r are assumed to be arranged on a cubic lattice (Fig. 8).^{25,26} The concept is similar to lattice models previously used to describe both the rubbery and glassy states.^{46,47} The average distance between neighboring holes is estimated from a mechanistic interpretation of E_D ,^{10,48–50} in which the energy required to create a channel of cross-sectional area $\pi d^2/4$ and diffusional jump length α is equated with the energy required to break the physical bonds between the polymer segments:

$$E_D = \frac{1}{4} \pi d^2 \alpha \text{ CED } N_A \quad (9)$$

where d is the collision diameter of the gas penetrant, CED is the cohesive energy density of the polymer, N_A is Avogadro's number, and E_D is determined by the Arrhenius relationship between D and T^{-1} . According to the concept expressed by eq 9, a similarity in the activation energies for diffusion obtained for various aromatic polyesters translates to similar α values of approximately 13.6 Å (Table 1). The corresponding radius of uniform spherical holes (r_m) follows from FFV:

$$r_m = \alpha \sqrt[3]{\frac{3 \text{ FFV}}{4\pi}} \quad (10)$$

where FFV is obtained from the oxygen solubility according to eq 8. The calculated hole radius (r_m) for various glassy polyesters correlates well with the hole size obtained independently by PALS (Table 1).^{25,26}

Furthermore, the hole density (N_0) in a cubic lattice is defined by the lattice constant, or α :

$$N_0 = \frac{1}{\alpha^3} \quad (11)$$

For the polymers in Table 1, N_0 from eq 11 varies from 3.6 to 4.6×10^{20} cm⁻³, which correlates with an N_0 value of about 4×10^{20} cm⁻³ determined for a range of polymers in various PALS studies, which considered either an average hole size^{51–53} or a distribution of hole sizes.⁵⁴

The consistency with independent estimates of the hole size and hole density supports the simple physical model that views gas diffusion as the random hopping of

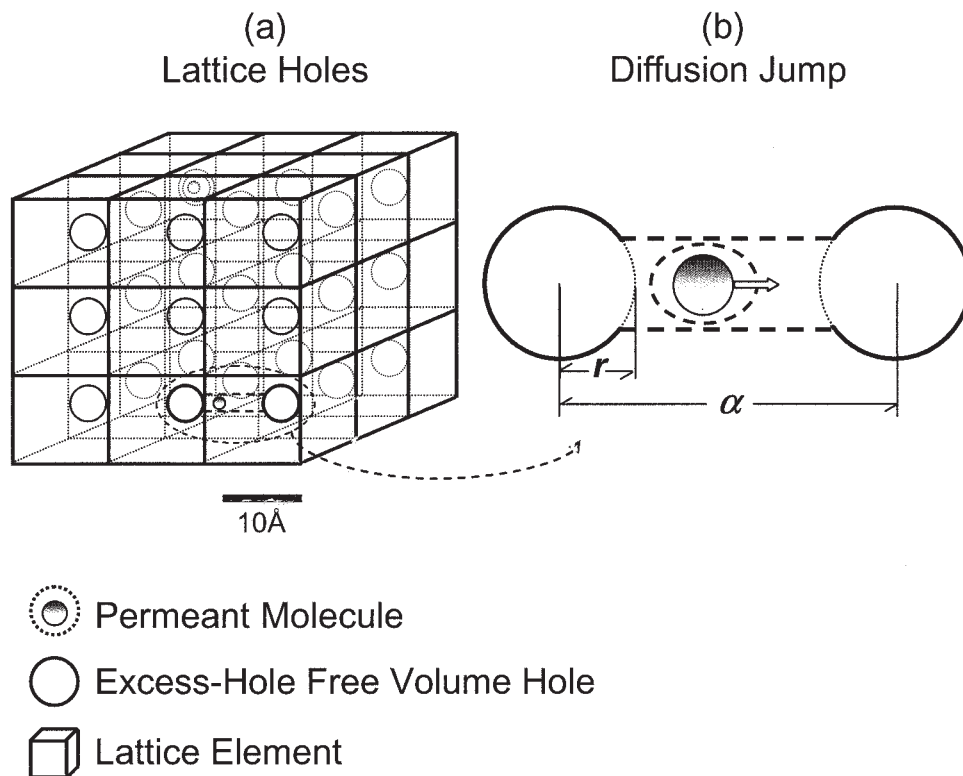


Figure 8. Lattice model for oxygen transport: (a) cubic lattice of excess free-volume holes and (b) diffusional jump of an oxygen molecule between free-volume holes.²⁵

an oxygen molecule from one excess-hole free volume hole to another. It should be emphasized, however, that this model applies under conditions in which only hole-filling sorption participates in the transport process.

From eq 9, the similarity in the E_D values of PET and PEN means that the low diffusivity of PEN cannot be ascribed to a difference in α . D depends on α and also on the effective jump frequency (ω):⁵⁵

$$D = \frac{1}{6} \omega \alpha^2 \quad (12)$$

It follows that the jump frequency is much lower in PEN and PEI. From D and α in Table 1, ω decreases from about $2.0 \times 10^6 \text{ s}^{-1}$ for PET and PETBB55 to $0.5 \times 10^6 \text{ s}^{-1}$ for PEI and PEN. For PET at 25 °C, this means that one oxygen molecule makes one jump every $5.3 \times 10^5 \text{ ps}$.²⁵ The timescale of the actual jump is on the order of several picoseconds from molecular simulations.⁵⁰ If the time spent in jumping is compared with the time spent in the hole, over 99% of the time is spent in the hole. This conforms to the understanding that gas molecules sorbed in the polymer glass reside mostly in the holes rather than in the matrix.^{25,29}

Only a small fraction of the holes contains an oxygen molecule at any given instant.²⁵ ρ_{O_2} in PET is $3.8 \times 10^{-3} \text{ g/cm}^3$ of excess-hole free volume at 25 °C and 1 atm. This is significantly smaller than the density of one gas molecule per hole, which would be 0.56 g/cm^3 of free volume estimated from a hole density of $4.0 \times 10^{20} \text{ cm}^{-3}$. The fraction of filled holes is estimated to be less than 1%. Nevertheless, if each permeant molecule jumps $0.5\text{--}2.0 \times 10^6$ times per second, all the holes will be probed many times over in 1 s. Although the number of gas molecules sorbed in the glassy state is considerably smaller than the number of accessible free-volume holes (<1%), the sorbed gas is seen as occupying all the free volume through a high jump frequency. The free-volume holes are interconnected by diffusion channels, which are instantly opened and closed by subambient segmental motion. The fast jump rate justifies the concept of sorbed gas density in eqs 4 and 6 because the gas molecules share all the free-volume holes.

Permeability of the LC Glass

Interpretations of the oxygen solubility and diffusivity based on free-volume concepts of the amorphous glass can be extended to the LC glass.^{26,43} PDEGGB is a

smectic LC glass with an oxygen permeability of 0.0318 cc (STP) cm m⁻² day⁻¹ atm⁻¹, which is more than one order of magnitude lower than the oxygen permeability of amorphous PET (Table 1). The exceptionally low oxygen permeability is due primarily to very low oxygen solubility. If the sorbed oxygen is in the same state (i.e., β in eq 5 applies to the smectic LC glass), FFV of PDEGBB from eq 8 is 0.005. In terms of the free-volume hole model, this means that the hole size is smaller or the hole density is lower than that of the amorphous glass. The smaller hole size of the LC glass is confirmed by PALS, which gives a hole radius of 2.23 Å for PDEGBB versus 2.56 Å for PET (Table 1). In addition, a higher E_D value for PDEGBB (53.4 kJ mol⁻¹) translates into a larger α value. The free-volume hole density estimated for PDEGBB is 1.7×10^{20} cm⁻³ according to eq 11, which is significantly lower than the hole density of about 4.0×10^{20} cm⁻³ obtained for the amorphous glasses. The FFV calculated from the hole size and hole density is 0.008, which is close to the value of 0.005 obtained directly from oxygen solubility (Table 1). Both the smaller hole size and lower hole density contribute to the lower FFV of the smectic LC glass.

CRYSTALLINE POLYESTERS

Oxygen Solubility and Glassy Amorphous Phase

The impermeability of crystals is the basis of the simple two-phase transport model, which consists of an impermeable crystal phase dispersed in a permeable amorphous matrix. The resulting relationship between the solubility and crystallinity volume is

$$S = S_a(1 - \phi_c) \quad (13)$$

where S_a is the solubility of the gas in the amorphous phase and ϕ_c is the volume fraction crystallinity. If S_a is independent of the amount of crystallinity and equal to the solubility of the completely amorphous polymer, S will decrease linearly with ϕ_c and extrapolate to zero solubility at $\phi_c = 1$. However, the solubility of many gases including oxygen in PET is significantly higher than that predicted by eq 13.⁵ An X-ray study suggests that the amorphous phase density (ρ_a) of crystalline PET is not constant but rather decreases with crystallinity because of conformational restrictions that change the ratio of amorphous gauche-to-trans conformers. The concept of a dedensified amorphous phase explains the unexpectedly high gas solubility of crystalline PET, PET copolymers, and PEN.^{20,56-58} The effect of crystallization on oxygen-transport properties is illustrated for PEN in Figure 9, with the crystallinity expressed as the density.⁵⁸ Crystallization has almost no effect on S , which

remains virtually constant at the value for amorphous PEN of 0.127 cc (STP) cm⁻³ atm⁻¹. A reduction in P by a factor of 3 in cold- and melt-crystallized PEN is due almost entirely to a decrease in D .

The two-phase model for the density of a crystallized polymer with a dedensified amorphous phase is formulated in terms of a crystalline phase of constant density (ρ_c) and an amorphous phase of variable density (ρ_a) that depends on ϕ_c :

$$\rho = \rho_c\phi_c + \rho_a(1 - \phi_c) \quad (14)$$

where ρ is the bulk density. To obtain ρ_a , ϕ_c is taken from the DSC heat of melting (ΔH):

$$\phi_c = \frac{\Delta H}{\Delta H^0} \frac{\rho}{\rho_c} \quad (15)$$

where ΔH^0 is the heat of melting of the perfect crystal. The relationship between S_a from eq 13 and the amorphous-phase specific volume ($\nu_a = \rho_a^{-1}$) from eq 14 with $\Delta H^0 = 131$ J g⁻¹ and $\rho_c = 1.445$ g cm⁻³ is plotted in Figure 10. The dedensification of the amorphous phase can be seen as a linear increase in S_a with increasing ν_a . The dashed line in Figure 10 is taken from Figure 6 and represents the decrease in S due to densification by orientation. Slope β and intercept ν_0 , which describe S of the densified oriented polymer, also describe S_a of the dedensified amorphous phase of the crystallized polymer. The orientation and crystallization both impact the amorphous state by altering the excess-hole free volume, although the effects are opposite: orientation reduces the free volume and crystallization increases the free volume. Analogous phenomena occur in PET, and the competing effects of simultaneous orientation and crystallization are manifest in the blown bottle wall.⁵⁹

The dedensification of the amorphous phase can be discussed in terms of the temperature–volume relationship in Figure 5.⁵⁸ As the polymer is cooled from the melt, unconstrained amorphous chains contract along the equilibrium liquid line to the glass transition and then along the solid line to 25 °C. However, amorphous chain segments that are attached to chain segments in crystals lack mobility to relax along the liquid line; instead, they are immobilized much as they would be in the glassy state, and during cooling from the crystallization temperature they contract along a line parallel to the glass line. The dashed lines in Figure 5 describe the contraction of the constrained amorphous phase from two different crystallization temperatures. In contrast to orientation, crystallization takes the amorphous phase further from equilibrium.

The additional free volume resulting from constraint is the difference between the dedensified amorphous specific volume of the completely crystallized polymer

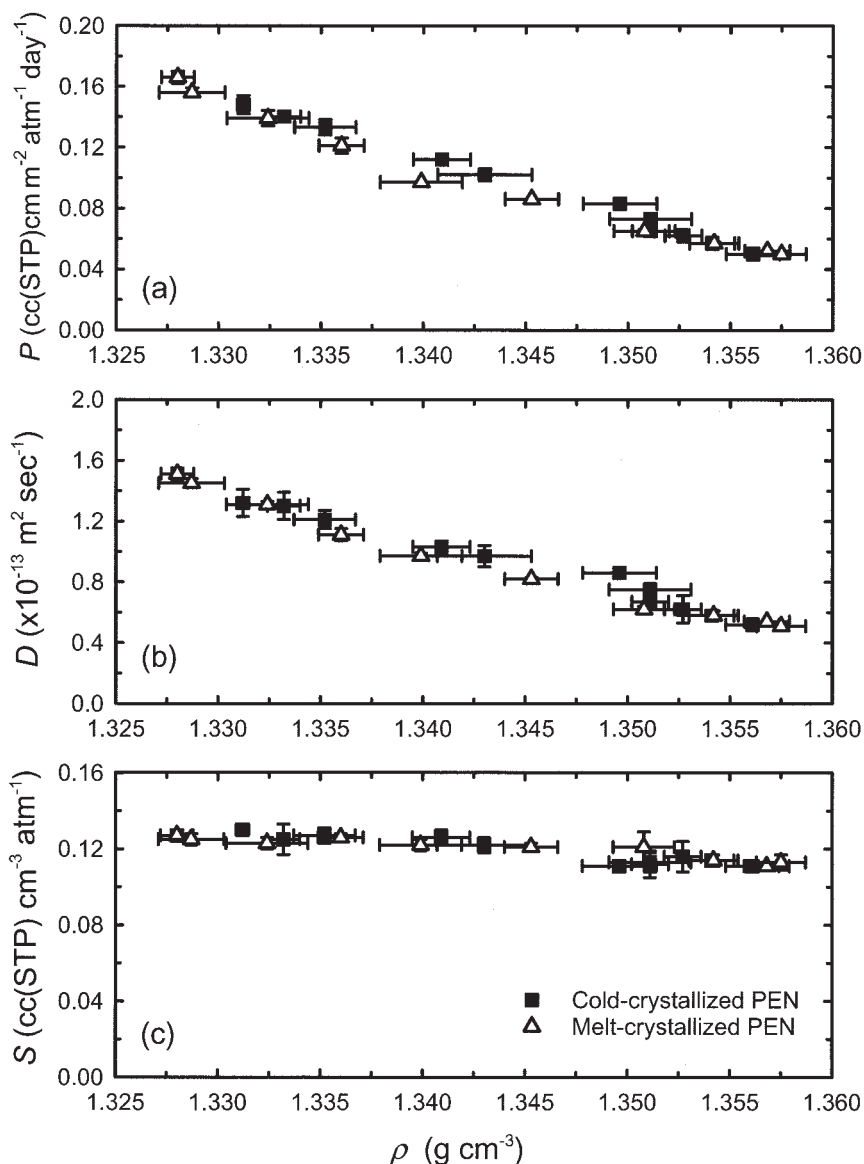


Figure 9. Effect of crystallinity expressed as ρ on the oxygen-transport parameters of PEN.⁵⁸ Reprinted with permission from Hu, Y. S.; Liu, R. Y. F.; Zhang, L. Q.; Rogunova, M.; Schiraldi, D. A.; Nazarenko, S.; Hiltner, A.; Baer, E. *Macromolecules* 2002, 35, 7326. Copyright 2002 American Chemical Society.

(ν_{\max}) and the specific volume of the unconstrained glass (ν_g). ν_{\max} is given by

$$\nu_{\max} = \nu_g + \Delta\nu_f = \nu_g + \Delta e(T_c - T_g) \quad (16)$$

where Δe is the difference between the specific thermal expansivities of equilibrium liquid and glass ($\Delta e = e_l - e_g$) and T_c is the crystallization temperature. The values of ν_{\max} calculated from eq 16 with literature values of e_l and e_g correlate well with ν of the dedensified amorphous phase obtained experimentally from the oxygen solubility.⁵⁸

Permeability and Microstructure of Spherulites

The isothermal crystallization of a polyester can be arrested before the spherulites are space-filling by quenching below T_g . The partially crystallized polyester can be viewed morphologically as a dispersion of spherulites in a continuous amorphous matrix (Fig. 11).^{58,60} However, the impermeable units are lamellar crystals, not spherulites. The individual spherulite is itself a composite structure consisting of impermeable lamellar crystals arranged in a permeable interlamellar amorphous phase with lower density than the amorphous matrix.

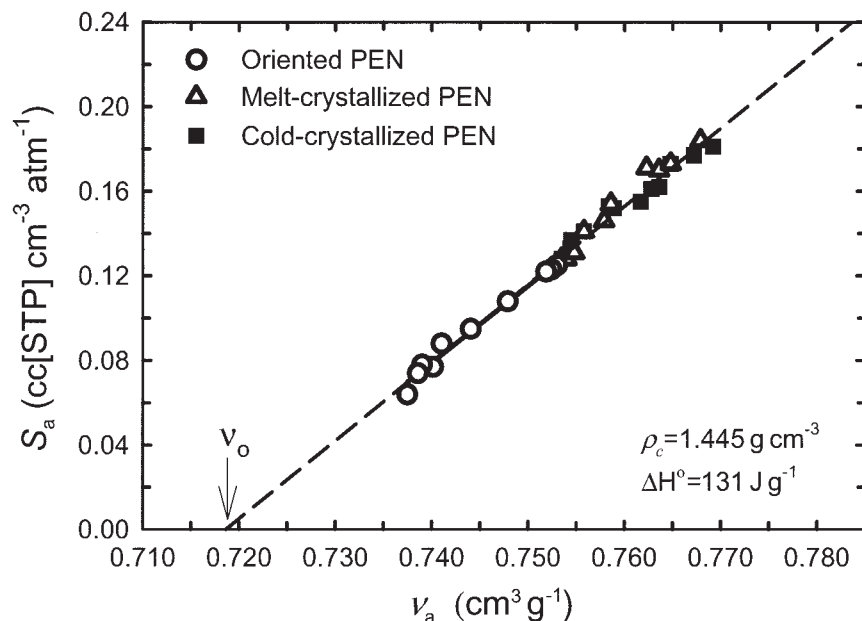


Figure 10. Relationship between S_a for oxygen and v_a for cold-crystallized and melt-crystallized PEN.⁵⁸ Reprinted with permission from Hu, Y. S.; Liu, R. Y. F.; Zhang, L. Q.; Rogunova, M.; Schiraldi, D. A.; Nazarenko, S.; Hiltner, A.; Baer, E. *Macromolecules* 2002, 35, 7326. Copyright 2002 American Chemical Society.

Although gas solubility is a powerful structural probe for the amorphous phase of a crystalline polyester, changes in the solubility are relatively small in comparison with the dramatic effect that the second phase can have on gas diffusivity (Fig. 9). The geometric impedance imparted to the transport pathway by a second phase is usually modeled in terms of gas permeability. Considering the crystallized polyester as a dispersion of less permeable spherulites in a more permeable amorphous matrix, the Maxwell model for the permeability of a spherical dispersion takes the following form:^{61–63}

$$P = P_a \left[1 + \frac{3V_s}{\left[\frac{(P_s/P_a) + 2}{(P_s/P_a) - 1} \right] - V_s} \right] \quad (17)$$

where V_s is the volume fraction of the spherulites, P_a is the permeability of the amorphous matrix, and P_s is the permeability of the spherulites and the single fitting parameter. The quantity P/P_a is plotted versus V_s in Figure 12 for PEN crystallized at two temperatures. The oxygen permeability of the spherulite is approximately 30–50% of that of the amorphous polymer. The lower P_s value of the spherulites crystallized at the higher temperature results from a higher volume fraction of impermeable lamellae and more than compensates for the lower interlamellar ρ_a value.

Structurally, the spherulite resembles a dispersion of impermeable platelets of a given aspect ratio, which was

modeled by Cussler and coworkers.^{64–66} If the platelet orientation is averaged, the permeability of the composite can be expressed as follows:

$$P_s = P_{as} \left[1 + \frac{\alpha^2 \phi_s^2}{12(1 - \phi_s)} \right]^{-1} \quad (18)$$

where P_{as} is the permeability of the dedensified interlamellar matrix, ϕ_s is the volume fraction of impermeable platelets, and α is the aspect ratio of the platelets. The resulting aspect ratio of the impermeable crystals is 18–20. The estimated lamellar length appears reasonable according to atomic force microscopy images.⁵⁸

Two-phase gas-transport models are also exceptionally useful for probing the morphology of polyesters that do not crystallize as well-formed spherulites. In this respect, gas permeability provides a valuable complement to more conventional methods such as X-ray diffraction, microscopy, and thermal analysis. For instance, the crystallization of PETBB55 from the melt reduces the oxygen permeability by a factor of 5. The effect is described well by a model that considers only a random dispersion of impermeable platelets in a permeable matrix,⁶⁶ and this corroborates the poor spherulitic development, loosely organized lamellae, and pronounced secondary crystallization of PETBB55.⁶⁷ Modeling the more modest effect of cold crystallization by heating the quenched PETBB55 glass above T_g leads to a consideration of small isotropic crystals embedded in a permeable

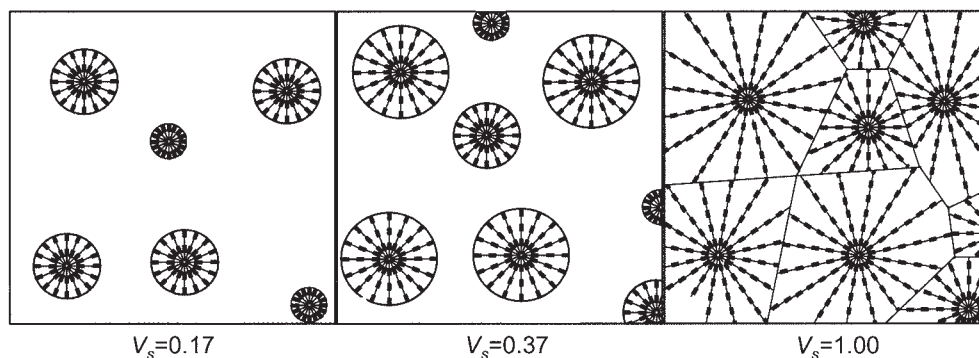


Figure 11. Schematic representation of compact banded spherulites at different time points during the isothermal crystallization of PEN.⁵⁸ Reprinted with permission from Hu, Y. S.; Liu, R. Y. F.; Zhang, L. Q.; Rogunova, M.; Schiraldi, D. A.; Nazarenko, S.; Hiltner, A.; Baer, E. *Macromolecules* 2002, 35, 7326. Copyright 2002 American Chemical Society.

matrix.^{43,67} Coincidentally, cold-crystallized PETBB55 exhibits an almost featureless, granular morphology despite the high level of crystallinity inferred from thermal analysis and X-ray diffraction. Similarly, an analysis of the oxygen permeability suggests that PDEGBB, an LCP, also crystallizes as small crystals with a low aspect ratio dispersed in the permeable LC phase, although there appears to be no morphological manifestation of crystalline order.⁴³

NEW OPPORTUNITIES FOR GAS TRANSPORT AS A STRUCTURE PROBE

Insight into the polymer amorphous phase is particularly elusive. Even in conventional polyolefins such as polypro-

pylene, the nature of the amorphous phase is not entirely understood, as evidenced by unresolved differences between the crystallinity measured by the density and the crystallinity measured by the heat of melting.⁶⁸ Various examples in this review illustrate how the transport of small gas molecules senses the permeable amorphous structure and probes the free volume of the disordered phase. This level of understanding has special practical importance for polyolefins for which environmental control is a key property in many packaging applications.

It is abundantly clear from the literature that elucidating solid-state structure–property relationships of complex polymeric materials requires the integration of insights from many experimental techniques. The chal-

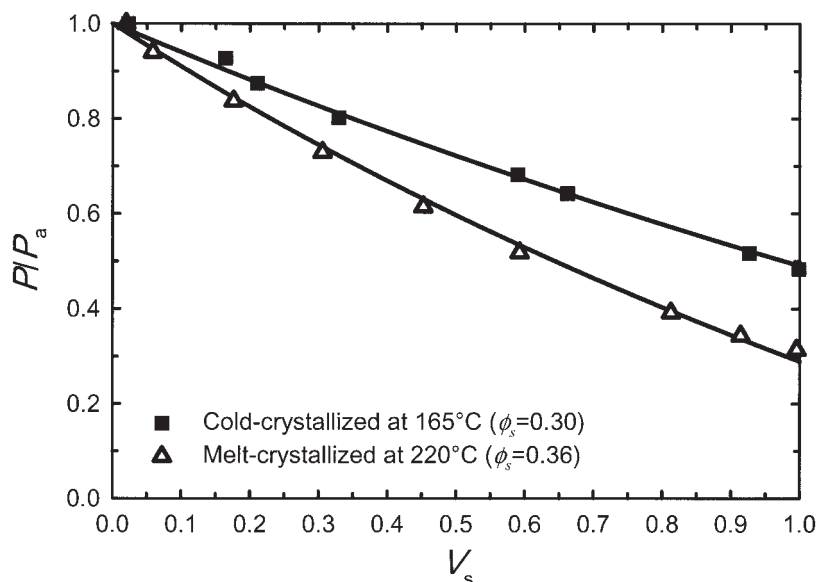


Figure 12. Relative permeability (P/P_a) versus V_s for cold-crystallized and melt-crystallized PEN and the fit to eq 17.⁵⁸ Reprinted with permission from Hu, Y. S.; Liu, R. Y. F.; Zhang, L. Q.; Rogunova, M.; Schiraldi, D. A.; Nazarenko, S.; Hiltner, A.; Baer, E. *Macromolecules* 2002, 35, 7326. Copyright 2002 American Chemical Society.

lenges are magnified by unusual solid-state structures, such as those of ionomers, including Nafion, a polymer that is of considerable current interest for fuel-cell applications.⁶⁹ Currently, polymer nanocomposites are the focus of many research efforts, which have provided ample evidence that even small amounts of high-aspect-ratio nanoparticles substantially impact solid-state properties, including gas transport.⁷⁰ Gas transport supplements more conventional methods for developing structural models of these unusual materials.

Current directions in microtechnology and nanotechnology frequently require the confinement of polymers as very thin films. As polymers become thinner, departures from the structure and properties of the bulk are expected.⁷¹⁻⁷³ The challenges of characterizing the small amounts of materials in nanofilms with conventional methods of polymer analysis are addressed by the multiplication of the number of thin films a 100-fold or even a 1000-fold by layer-multiplying coextrusion.^{74,75} The scientifically and technologically important interphase between two immiscible polymers is probed with assemblies of thousands of alternating layers of two glassy polymers, with the individual layer thickness on the nanometer size scale of the interphase.^{76,77} By sensing the composite nature of the assembly, gas transport becomes a primary method for extracting the dimension and other fundamental characteristics of the interphase. Nanolayer assemblies of crystalline polymers are also fabricated by layer-multiplying coextrusion. Confinement on the nanoscale impacts nucleation and growth to the extent that new crystalline structures are created.^{78,79} The gas-transport parameters of solubility and diffusivity are sensitive probes for the new and unique solid-state structures of ultrathin polymers.

This research was generously supported by the National Science Foundation (DMR-0349436), the Defense Advanced Research Projects Agency (DARPA) (MDA972-02-1-0011), and INVISTA.

REFERENCES AND NOTES

1. Michaels, A. S.; Bixler, H. J. *J Polym Sci* 1961, 50, 413.
2. Rogers, C. E. In *Polymer Permeability*; Comyn, J., Ed.; Elsevier: London, 1985; Chapter 2, pp 11-74.
3. Vieth, W. R. *Diffusion in and through Polymers: Principles and Applications*; Oxford University Press: Munich, 1991; Chapter 1, pp 1-14.
4. Barrer, R. M.; Barrie, J. A.; Slater, J. *J Polym Sci* 1958, 27, 177.
5. Michaels, A. S.; Vieth, W. R.; Barrie, J. A. *J Appl Phys* 1963, 34, 1.
6. Michaels, A. S.; Bixler, H. J.; Fein, H. J. *J Appl Phys* 1964, 35, 3165.
7. Koros, W. J.; Paul, D. R. *J Polym Sci Polym Phys Ed* 1978, 16, 1947.
8. Koros, W. J.; Paul, D. R. *J Polym Sci Polym Phys Ed* 1981, 19, 1655.
9. Barbari, T. A.; Koros, W. J.; Paul, D. R. *J Polym Sci Part B: Polym Phys* 1988, 26, 729.
10. Meares, P. *J Am Chem Soc* 1954, 76, 3415.
11. Chiou, J. S.; Paul, D. R. *J Polym Sci Part B: Polym Phys* 1987, 25, 1699.
12. Weinkauff, D. H.; Paul, D. R. In *Barrier Polymers and Structures*; Koros, W. J., Ed.; American Chemical Society: Washington, DC, 1990; Chapter 3, pp 60-91.
13. Weinkauff, D. H.; Paul, D. R. *J Polym Sci Part B: Polym Phys* 1992, 30, 817.
14. Slee, J. A.; Orchard, G. A. J.; Bower, D. I.; Ward, I. M. *J Polym Sci Part B: Polym Phys* 1989, 27, 71.
15. Orchard, G. A. J.; Spiiby, P.; Ward, I. M. *J Polym Sci Part B: Polym Phys* 1990, 28, 603.
16. Taraiya, A. K.; Orchard, G. A. J.; Ward, I. M. *J Polym Sci Part B: Polym Phys* 1993, 31, 641.
17. Weigmann, H. D.; Scott, M. G.; Ribnick, A. S.; Matkowsky, R. D. *Text Res J* 1977, 47, 745.
18. Makarewicz, P. J.; Wilkes, G. L. *J Polym Sci Polym Phys Ed* 1978, 16, 1529.
19. Serad, G. E.; Freeman, B. D.; Stewart, M. E.; Hill, A. J. *Polymer* 2001, 42, 6929.
20. Sekelik, D. J.; Stepanov, S. V.; Nazarenko, S.; Schiraldi, D.; Hiltner, A.; Baer, E. *J Polym Sci Part B: Polym Phys* 1999, 37, 847.
21. Crank, J. *The Mathematics of Diffusion*; Clarendon: Oxford, 1956.
22. Vrentas, J. S.; Duda, J. L. *J Appl Polym Sci* 1978, 22, 2325.
23. Liu, R. Y. F.; Schiraldi, D. A.; Hiltner, A.; Baer, E. *J Polym Sci Part B: Polym Phys* 2002, 40, 862.
24. Polyakova, A.; Liu, R. Y. F.; Schiraldi, D. A.; Hiltner, A.; Baer, E. *J Polym Sci Part B: Polym Phys* 2001, 39, 1889.
25. Liu, R. Y. F.; Hiltner, A.; Baer, E. *J Polym Sci Part B: Polym Phys* 2004, 42, 493.
26. Hu, Y. S.; Liu, R. Y. F.; Schiraldi, D. A.; Hiltner, A.; Baer, E. *Macromolecules* 2004, 37, 2136.
27. Merkel, T. C.; Freeman, B. D.; Spontak, R. J.; He, Z.; Pinnau, I.; Meakin, P.; Hill, A. J. *Science* 2002, 296, 519.
28. Weiss, G. H.; Bendler, J. T.; Shlesinger, M. F. *Macromolecules* 1992, 25, 990.
29. Theodorou, D. N. In *Diffusion in Polymers*; Neogi, P., Ed.; Marcel Dekker: New York, 1996; Chapter 2, pp 67-142.
30. Stern, S. A. *J Membr Sci* 1994, 94, 1.
31. Polyakova, A.; Connor, D. M.; Collard, D. M.; Schiraldi, D. A.; Hiltner, A.; Baer, E. *J Polym Sci Part B: Polym Phys* 2001, 39, 1900.
32. Van Krevelen, D. W. *Properties of Polymers*, 3rd ed.; Elsevier: Amsterdam, 1997; Chapter 4, pp 71-107.

33. Gibbs, J. H.; DiMarzio, E. A. *J Chem Phys* 1958, 28, 373.
34. Miller, A. A. *J Polym Sci Part A: Gen Pap* 1963, 1, 1857.
35. Ferry, J. D. *Viscoelastic Properties of Polymers*, 3rd ed.; Wiley: New York, 1980; Chapter 11, pp 264–320.
36. Qureshi, N.; Stepanov, E. V.; Schiraldi, D.; Hiltner, A.; Baer, E. *J Polym Sci Part B: Polym Phys* 2000, 38, 1679.
37. Ma, H. M.; Hibbs, M.; Collard, D. M.; Kumar, S.; Schiraldi, D. A. *Macromolecules* 2002, 35, 5123.
38. Light, R. R.; Seymour, R. W. *Polym Eng Sci* 1982, 22, 857.
39. Ezquerra, T. A.; Balta-Calleja, F. J.; Zachmann, H. G. *Acta Polym* 1993, 44, 18.
40. Muruganandam, N.; Koros, W. J.; Paul, D. R. *J Polym Sci Part B: Polym Phys* 1987, 25, 1999.
41. Walton, J. H.; Lizak, M. J.; Conradi, M. S.; Gullion, T.; Schaefer, J. *Macromolecules* 1990, 23, 416.
42. Berticat, P.; Chatain, D.; Monpagens, J. C.; Lacabanne, C. *J Macromol Sci Phys* 1978, 15, 549.
43. Hu, Y. S.; Schiraldi, D. A.; Hiltner, A.; Baer, E. *Macromolecules* 2003, 36, 3606.
44. Andrade, G. S.; Collard, D. M.; Schiraldi, D. A.; Hu, Y. S.; Baer, E.; Hiltner, A. *J Appl Polym Sci* 2003, 89, 934.
45. Uralil, F.; Sederel, W.; Anderson, J. M.; Hiltner, A. *Polymer* 1979, 20, 51.
46. Rane, S.; Gujrati, P. D. *Phys Rev E* 2001, 64, 011801.
47. Simha, R.; Somcynsky, T. *Macromolecules* 1969, 2, 342.
48. Thran, A.; Kroll, G.; Faupel, F. *J Polym Sci Part B: Polym Phys* 1999, 37, 3344.
49. Duda, J. L.; Zielinski, J. M. In *Diffusion in Polymers*; Neogi, P., Ed.; Marcel Dekker: New York, 1996; Chapter 3, pp 143–172.
50. Takeuchi, H. *J Chem Phys* 1990, 93, 2062.
51. Srithawatpong, R.; Peng, Z. L.; Olson, B. G.; Jamieson, A. M.; Simha, R.; McGervey, J. D.; Maier, T. R.; Halasa, A. F.; Ishida, H. *J Polym Sci Part B: Polym Phys* 1999, 37, 2754.
52. Bamford, D.; Dlubek, G.; Reiche, A.; Alam, M. A.; Meyer, W.; Galvosas, P.; Rittig, F. *J Chem Phys* 2001, 115, 7260.
53. Dlubek, G.; Bondarenko, V.; Pionteck, J.; Supej, M.; Wutzler, A.; Krause-Rehberg, R. *Polymer* 2003, 44, 1921.
54. Hong, X.; Jean, Y. C.; Yang, H. J.; Jordan, S. S.; Koros, W. J. *Macromolecules* 1996, 29, 7859.
55. Petropoulos, J. H. In *Polymeric Gas Separation Membranes*; Paul, D. R.; Yampol'ski, Y. P., Eds.; CRC: Boca Raton, FL, 1994; Chapter 2, pp 17–82.
56. Polyakova, A.; Stepanov, E. V.; Sekelik, D.; Schiraldi, D. A.; Hiltner, A.; Baer, E. *J Polym Sci Part B: Polym Phys* 2001, 39, 1911.
57. Lin, J.; Shenogin, S.; Nazarenko, S. *Polymer* 2002, 43, 4733.
58. Hu, Y. S.; Liu, R. Y. F.; Zhang, L. Q.; Rogunova, M.; Schiraldi, D. A.; Nazarenko, S.; Hiltner, A.; Baer, E. *Macromolecules* 2002, 35, 7326.
59. Liu, R. Y. F.; Hu, Y. S.; Schiraldi, D. A.; Hiltner, A.; Baer, E. *J Appl Polym Sci* 2004, 94, 671.
60. Hu, Y. S.; Rogunova, M.; Schiraldi, D. A.; Hiltner, A.; Baer, E. *J Appl Polym Sci* 2002, 86, 98.
61. Petropoulos, J. H. *Adv Polym Sci* 1985, 64, 93.
62. Barrer, R. M. In *Diffusion in Polymers*; Crank, J., Park, G. S., Eds.; Academic: New York, 1968; Chapter 6, pp 165–217.
63. Puleo, A. C.; Paul, D. R.; Wong, P. K. *Polymer* 1989, 30, 1357.
64. Cussler, E. L.; Hughes, S. E.; Ward, W. J.; Aris, R. *J Membr Sci* 1988, 38, 161.
65. Eitzman, D. M.; Melkote, R. R.; Cussler, E. L. *AIChE J* 1996, 42, 2.
66. Falla, W. R.; Mulski, M.; Cussler, E. L. *J Membr Sci* 1996, 119, 129.
67. Hu, Y. S.; Liu, R. Y. F.; Rogunova, M.; Schiraldi, D. A.; Nazarenko, S.; Hiltner, A.; Baer, E. *J Polym Sci Part B: Polym Phys* 2002, 40, 2489.
68. Isasi, J. R.; Mandelkern, L.; Galante, M. J.; Alamo, R. G. *J Polym Sci Part B: Polym Phys* 1999, 37, 323.
69. Rikukawa, M.; Sanui, K. *Prog Polym Sci* 2000, 25, 1463.
70. Giannelis, E. P.; Krishnamoorti, R.; Manias, E. *Adv Polym Sci* 1999, 138, 107.
71. Sharma, A.; Reiter, G. *J Colloid Interface Sci* 1996, 178, 383.
72. Jérôme, B.; Commandeur, J. *Nature* 1997, 386, 589.
73. Forrest, J. A.; Dalnoki-Veress, K. *J Polym Sci Part B: Polym Phys* 2001, 39, 2664.
74. Baer, E.; Kerns, J.; Hiltner, A. In *Structure Development during Polymer Processing*; Cunha, A. M.; Fakirov, S., Eds.; Kluwer Academic: Dordrecht, 2000; pp 327–344.
75. Mueller, C.; Kerns, J.; Ebeling, T.; Nazarenko, S.; Hiltner, A.; Baer, E. In *Polymer Process Engineering 97*; Coates, P. D., Ed.; Institute of Materials: London, 1997; pp 137–157.
76. Liu, R. Y. F.; Jin, Y.; Hiltner, A.; Baer, E. *Macromol Rapid Commun* 2003, 24, 943.
77. Liu, R. Y. F.; Bernal-Lara, T. E.; Hiltner, A.; Baer, E. *Macromolecules* 2004, 37, 6972.
78. Pan, S. J.; Im, J.; Hill, M. J.; Keller, A.; Hiltner, A.; Baer, E. *J Polym Sci Part B: Polym Phys* 1990, 28, 1105.
79. Jin, Y.; Rogunova, M.; Hiltner, A.; Baer, E.; Nowacki, R.; Galeski, A.; Piorkowska, E. *J Polym Sci Part B: Polym Phys* 2004, 42, 3380.